J Sol-Gel Sci Technol (2011) 60:299–314
DOI 10.1007/s10971-011-2562-0

ORIGINAL PAPER

Hybrid organic–inorganic sol–gel materials for micro and nanofabrication

Giovanna Brusatin · Gioia Della Giustina

Received: 14 April 2011 / Accepted: 5 August 2011 / Published online: 8 September 2011

Abstract In this review hybrid organic–inorganic (HOI) resists as emerging materials alternative to organic polymers for micro and nanolithography are presented and discussed. In particular, results on sol–gel materials belonging to 3-glycidoxypropyltrimethoxysilane based HOI are presented and reviewed, highlighting as various lithographic techniques can be used to pattern their surface and showing examples of micro- and nano-patterned structures achieved with radiation assisted lithography (UV, X-rays and electron beam) or imprint techniques. It will be demonstrated the particular versatility shown by some of these materials, that in some case can be processed with all the lithographic methods herein considered, without any significant modification of their main composition and synthesis procedure. Moreover, results about the investigation of interaction between radiation and HOI materials and thermal treatment will be discussed, as well as possible synthesis strategies and composition modification developed in order to improve efficiency of curing, tailor HOI properties to specific needs (optical properties, resist composition, mechanical stability, etc.) and explore innovative and non conventional patterning techniques. The reported results highlight as these novel materials, thanks to their solution processability and higher performances respect to commercial polymeric resists, allow to use the above mentioned lithographic techniques in a direct patterning process, strongly simplifying conventional technique and reducing their processing time and costs.

G. Brusatin (✉) · G. Della Giustina
Department of Mechanical Engineering, Materials Section, University of Padova, Via Marzolo 9, 35131 Padova, Italy
e-mail: giovanna.brusatin@unipd.it

Keywords Hybrid organic–inorganic materials · Sol–gel · Glycidoxypropyltrimethoxysilane · Nanoimprinting · UV lithography · X-rays · Electron beam lithography

1 Introduction

The standard materials in the lithographic field are polymer based and generally used as sacrificial resist films. Existing conventional micro- and nano-fabrication technology is using complex multi-step processes involving resist deposition on the film to be patterned, lithography and etching. Therefore, the fine pattering of a thin film is often complex and represents a crucial processing step in most device fabrication, becoming a barrier for mass-production of devices requiring micro- or nano-fabrication especially when large etch depth and aspect ratio is required.

The possibility of using the resist material itself as final patterned film, instead of using etch transfer techniques, would be very attractive, taking advantage from its easy solution process. However, due to the relatively low performance and instability of polymeric materials to frequent operational and environmental conditions and limited range of properties, hybrid organic–inorganic (HOI) resists are emerging as an alternative to organic polymers for micro and nanolithography, having both solution processability together with higher performance, stability and wider choice of properties [1–7]. In particular, thermal resistance (<300 °C), mechanical strength (antiscratch) and chemical endurance (dissolution) typical of polymers can be improved by using HOI resists. Furthermore, the problem of "unknown chemistry" typical of commercial organic resists can be overcome allowing, for example, to dope the patternable film with organic dyes, nanoparticles

or other organic and inorganic species; the optical properties such as refractive index and resist porosity can be tuned, etc., allowing to use HOI resists like materials as integral part of a devices and to overcome the frequent inadequacy of commercial organic resists. Even more important, the use of HOI allows a huge simplification of traditional lithographic processes using sacrificial resists for the realization of devices requiring micro- or nano-patterning and several lithographic steps.

Among the more important conventional lithographic techniques are electron beam and X-rays lithography (EBL and XRL, respectively), that allow to achieve high pattern structures resolutions [8–11].

Most important non conventional techniques are thermal and UV assisted imprinting lithographies (T-NIL and UV-NIL, respectively) that are today considered very promising for their high throughput and obtainable resolution [12–15].

Concerning HOI resists, several HOI materials have already been reported in literature since few decades, as directly writable materials; the main part of it concerns UV sensitive HOI mainly methacrylate based, for the production of waveguides [16–22] and few other products [23–25] by using mask assisted UV lithography techniques (UVL) and UV Laser Interferential Lithography (UV-LIL).

This review resumes published results and some recent unpublished achievements on versatile HOI materials, based on 3-glycidoxypropyltrimethoxysilane (GPTMS, Scheme 1), developed by the authors to produce micro- and nano-patterned surfaces by direct writing with the five lithographic techniques above mentioned (UVL, UV-LIL, EBL, XRL and NIL, Fig. 1). In particular, results about the investigation of the interaction between radiation and HOI materials will be presented. Moreover, it will be underlined the particular versatility shown by some of these materials, that in some case can be processed with all the lithographic methods herein considered, without any significant modification of their main composition and synthesis procedure. Examples of different HOI patterned structures and properties, that can be obtained varying pattern techniques and compositions, will be shown.

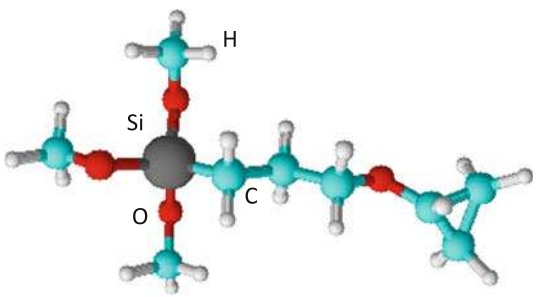

Scheme 1 3-Glycidoxypropyltrimethoxysilane, GPTMS

Hence, this study aims to give a better insight into alternative materials which can be used with lithographic techniques and into materials structure modification that these processes induce, highlighting the advantage of using a coupled bottom-up and top-down approach, i.e. sol–gel HOI materials synthesis and the lithographies above mentioned, to the realization of direct nano- and micro-patterned films.

1.1 Hybrid organic–inorganic materials (HOI) based on GPTMS

The studied HOI systems are based on 3-glycidoxypropyltrimethoxysilane (GPTMS, Scheme 1, 2) with the possible addition of different inorganic oxide precursors, in particular Si tetramethoxide (TMOS), Ge tetraethoxide (TEOG), Zr butoxide (ZrBut) and Ti propoxide (TiProp) for SiO_2, GeO_2, ZrO_2 and TiO_2 sol–gel synthesis, respectively.

Although HOI systems based on GeO_2, ZrO_2 and TiO_2 and acrylate as polymerizable functionalities are probably the most studied photopatternable materials for direct fabrication of micro-optical elements and optical waveguide [26–32], the use of HOI films bearing epoxy functionality as directly patternable materials is rarely investigated. Moreover, the few studies present in literature are focused on lithographies using UV light, while direct micro and nano patterning by EBL [33, 34], XRL [35–37] and NIL [5, 38–40] is less frequently reported.

One of the main reason for this is the difficulty of preserving epoxy functionality during the sol–gel synthesis in presence of tetrafunctional alkoxides different from Si ones and with a strong behavior as Lewis acid, such as the above mentioned transition metal precursors.

However, epoxy based HOI offers a few important properties with respect to acrylate based HOI, that will be highlighted in the examples below. The first is a high thermal stability of un-polymerized epoxies and UV transparency, because the cationic polymerization mechanism, used in the herein described works of the authors, is not inhibited by the presence of oxygen and cannot be started only by the temperature as in the case of radical processes widely used with acrylates [41, 42]. Moreover, high pattern resolution achievable with EBL or XRL will be demonstrated, that with the exception of a few examples of inorganic oxide based resists [3, 8, 33], represents an uncommon and outstanding result. Finally, one of the characteristic features, that is fundamental for the improvement of the just mentioned spatial resolution and the dimensional stability, is the limited shrinkage during polymerization typical of epoxy based HOI. Besides all this, it has to be pointed out the versatility of these materials, that can be directly patterned with a wide range of lithographic techniques.

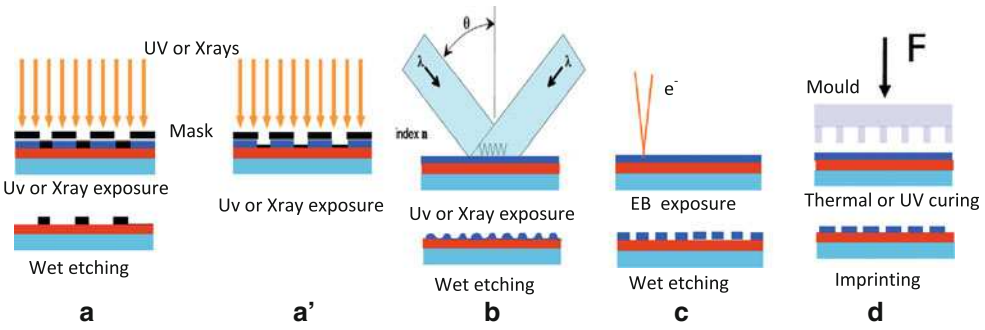

Fig. 1 Schemes of mask assisted UV lithography with (**a**) or without (**a′**) development step—the radiation is UV or X-rays; UV-LIL (**b**) EBL (**c**); NIL, UV or thermally assisted (**d**)

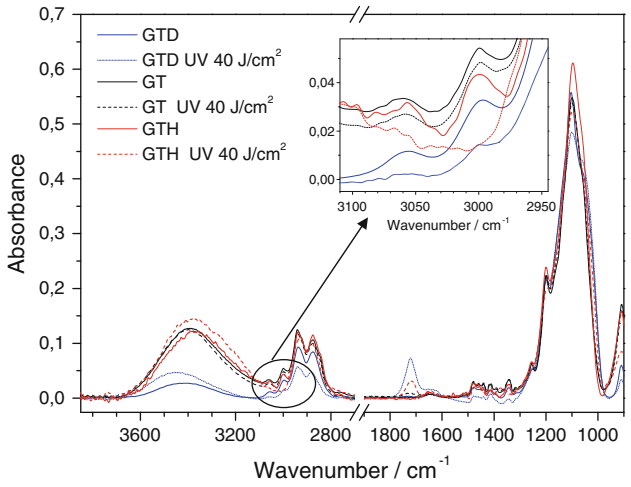

Fig. 2 FTIR spectra of GTD (1% DIC), GT and GTH (0.1% HPPF) films dried and irradiated with 40 J/cm^2 UV power density in the regions 3,850–2,700 and 1,900–900 cm^{-1}

Early studies on GPTMS based materials performed in our lab have been dedicated to improving their photosensitivity, by using cationic photo-initiators and to directly pattern these films with easy and fast production of channel waveguides. Different types of photoinitiators, necessary to make the resist photosensitive to UV radiation, were studied, with the aim to shorten as much as possible the UV exposure time and simultaneously set up thermally stable structures.

A summary of the main achievements in this direction are reported in the following. A simple system of GPTMS co-hydrolysed with Tetramethoxysilane (TMOS, molar ratio 70:30 reacted in acidic conditions with HCl/H_2O/TMOS = 0.008/2/1, the system is named GPTMS-SiO_2) is doped with different types of photoinitiators named DIC, HPPF and DPST (Scheme 3) and subjected to UV exposure with a Hamamatsu LC5 UV Hg(Xe) lamp. As shown by FTIR spectra of the irradiated GPTMS-SiO_2 films undoped (GT), doped with 1% DIC (GTD) and with 0.1% HPPF (GTH), the polymerization is not completed with 1% DIC (curves GTDUV40 J/cm^2), while the film seems to be completely polymerized at the same power density using 0.1% HPPF (curves GTDUV40 J/cm^2), indicating a different efficiency as cationic photoinitiator (Fig. 2).

In fact, despite the absorption of both DIC and HPPF peaks around 250 nm, the absorption intensity of HPPF is enhanced due to the presence of an electro donor alkoxy group linked to the benzenic ring [43]. The presence of the initiator causes a secondary damage effect in the organic structure of the film, evidenced by the increase of a band at 1,720 cm^{-1}, related to the formation of carbonyl hydrophilic groups and more pronounced when a less efficient initiator, such as DIC in this case, is used.

However, HPPF is thermally active as well and initiates the polymerization already at around 100 °C and a complete curing at 140 °C (film GTH in Fig. 3b); instead, the thermal treatment at 150 °C of DIC containing films

Scheme 2 Outline of the epoxy polymerization process owing to hybrid film exposure. From ref [38]

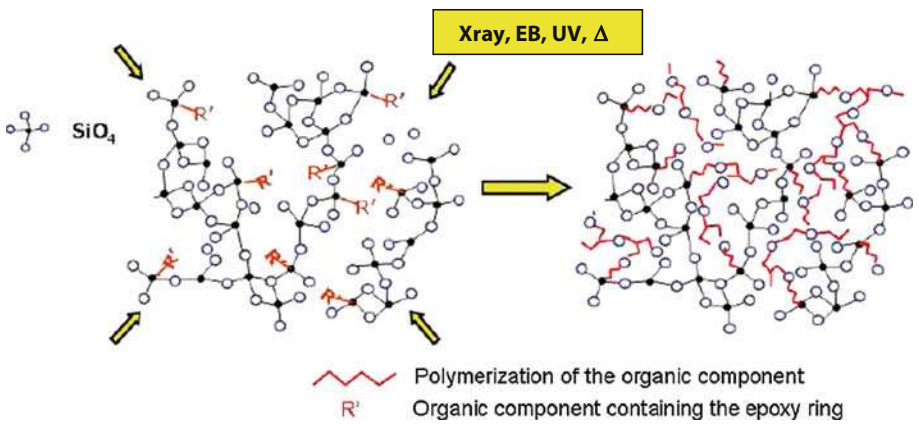

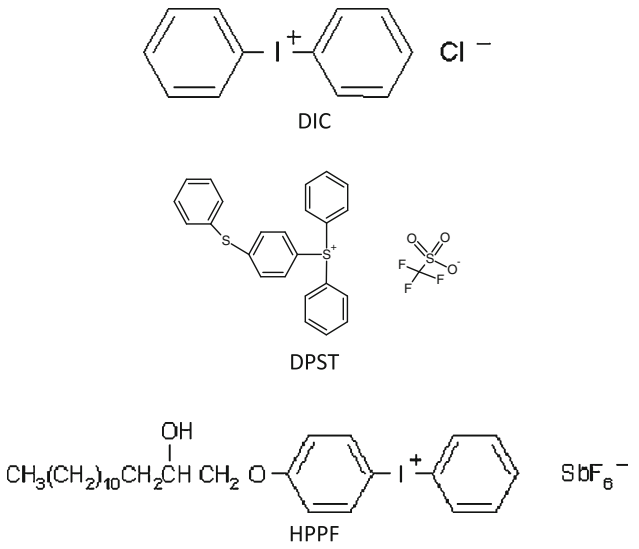

Scheme 3 Three different cationic photoinitiators tested. The absorption is centred at 250 nm (DIC), 250 nm (HPPF), 300 nm (DPST)

doesn't show any polymerization evidence (film GTD in Fig. 3a).

The exploitation of these directly patternable films for the production of micro-structures, for example channel waveguides, in short exposure times as those required by GTH system, but are also thermally stable to avoid channel waveguide definition loss upon thermal stresses, as in the case of GTD, requires efficient photoinitiators that at the same time preserve epoxy from thermal polymerization.

The above mentioned problems were overcome by using the photoinitiator DPST (Scheme 3), that has a greater photolytic efficiency with respect to other photoacid generators [44] due to its extended conjugation resulting from the presence of the 4-thiophenoxy chromophore. In particular, DPST was compared with DIC and it was found to get a more efficient photopolymerization, producing a complete curing with initiator concentration ten times smaller than DIC and lower UV doses. Figure 4 show these results, on a system based on GPTMS and co-hydrolysed with Ge ethoxide (GPTMS-GeO_2) described below and reported in [45]. In the Fig. 4 the polymerization degree is represented by plotting the intensity of the epoxy vibration absorption at 3,060 cm^{-1}, normalized to the initial area, as a function of the irradiation time, for the same film containing 1% DIC or DPST as initiator: it can be seen that with DPST the complete polymerization is reached after 2 min, although the molar concentration of photoinitiator is the same.

1.2 HOI materials based on GPTMS-GeO_2

A low amount of GeO_2 (<30%) and the use of a synthesis process that preserves epoxy groups, allow to exploit

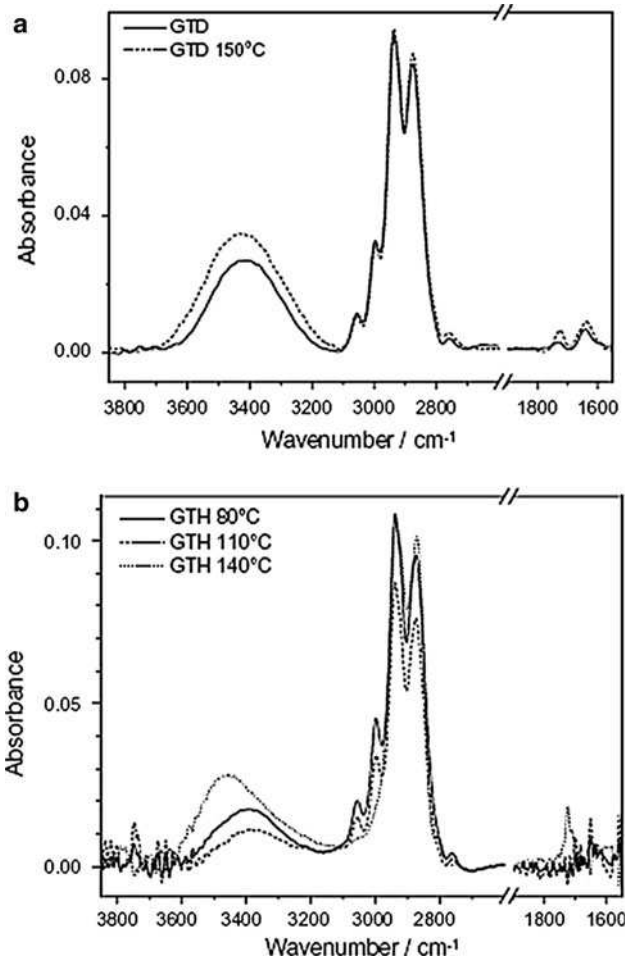

Fig. 3 FTIR spectra of **a** GTD (1% DIC) and **b** GTH (0.5% HPPF) films treated at different temperatures for 30 min. From ref [47]

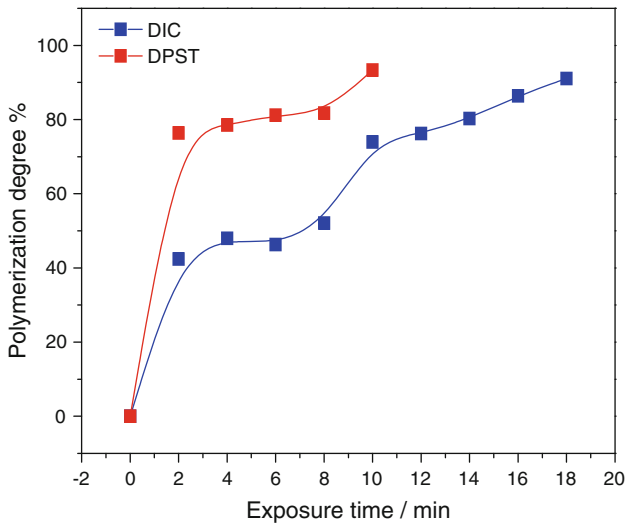

Fig. 4 Example of efficiency for GPTMS-GeO_2 film doped with different cationic photoinitiators, DIC (1 mol%) and DPST (1 mol%). 1 min irradiation corresponds to 15 J/cm^2

polymerization of such functionalities to direct pattern GPTMS-GeO_2 based films [46–48] (Scheme 2). In the earlier UVL experiments, HOI synthesized with GPTMS and TEOG in different amount (Ge/Si molar ratio between 0 and 3) have been explored for UVL. A basic synthesis was used with the highest amount of TEOG, as reported by the authors [45–47], to avoid epoxy opening by the Ge alkoxide which acts as Lewis acid. Figure 5a and b show channel waveguides fabricated by UV illumination of DPST doped films through a quartz slide with a chromium mask with open stripes of different sizes (4, 6, 8, 16 and 32 μm). After exposure, the unexposed zones were dissolved by a mixed solution of water/acetone in ratio 1:1 for 30 s. Figure 4 shows the degree of photopolymerization versus UV curing time, measured by the decreasing of the epoxy vibration absorption at 3,060 cm^{-1} that demonstrates the ring opening reaction.

Alternatively, the structures can be used without any development step after UV exposure, greatly simplifying the patterning process; an example of these structures is shown in Fig. 5c. In fact, the refractive index of the films changes consistently upon irradiation and the variation between exposed and unexposed part, of about 0.015 (not shown, [45]), is sufficient to ensure a good optical light confinement to produce waveguiding structures.

As previously mentioned, the use of an efficient cationic photoinitiator, that at the same time preserve epoxy from thermal polymerization, represents a real advantage of using epoxy based HOI in directly patterned micro optical structures; in fact, acrylate based polymers or HOI spontaneously undergo to thermal or self initiated polymerization, which would degrade the topology and refractive index.

Recently, we apply UV laser interference lithography (UV-LIL), an emerging and promising technology for the realization of large area 1D and 2D structures on photosensitive materials. This technique allows the fabrication of periodic patterns, of the order of 100 nm, using UV lasers in a single step on photosensitive materials. In particular, the use of HOI systems has been explored by the authors [49], on the GPTMS-GeO_2 films (Si/Ge = 8/2), by using DPST as photoinitiator and the two-beam interference excitation of a 50 mW HeCd laser ($\lambda = 325$ nm, KIMMON Koha-Model IK3501R-G). After post-exposure bake at 60 °C, the unexposed regions were dissolved by means of a diluted NaOH solution (NaOH: H_2O = 1:100). Examples of the generated sinusoidal light intensity pattern are shown in the AFM images of Fig. 6.

The advantage of using HOI sol–gel materials in the fabrication of sinusoidal gratings, respect to polymeric resists, lies in the higher control of both optical and geometrical parameters and in the realization of smother structures; by this way, the surface quality is improved and it is possible to match the properties of the patterned film, such as refractive index, chemical and mechanical resistance. This last feature is important, for example, if the same periodic relief patterns would be exploited as master itself, thanks to its higher rigidity respect to usual polymeric resists, or in the replica moulding technique.

A similar HOI GPTMS-GeO_2 system was used in XRL experiments [38, 46], synthesized from GPTMS and TEOG with a Ge/Si molar ratio of 2/8; in this case it was found that the films can be patterned without the addition of any photo-initiator, by exposing the film to a synchrotron radiation X-ray beam through a test mask and delivering a total dose of 2 J cm^{-2} in the range of photon energies of 1–2 keV. Again, in the exposed material epoxy functionalities polymerize and the film becomes hard and insoluble, while unexposed areas remain soft and soluble and can be dissolved (Shipley MF-322) providing a negative resist-like behaviour of the film. The absence of any initiator enhances the hardening difference between exposed and unexposed areas, thus improving the final lithographic contrast. Figure 7a and b show an example of pattern achieved by XRL, as previously summarized.

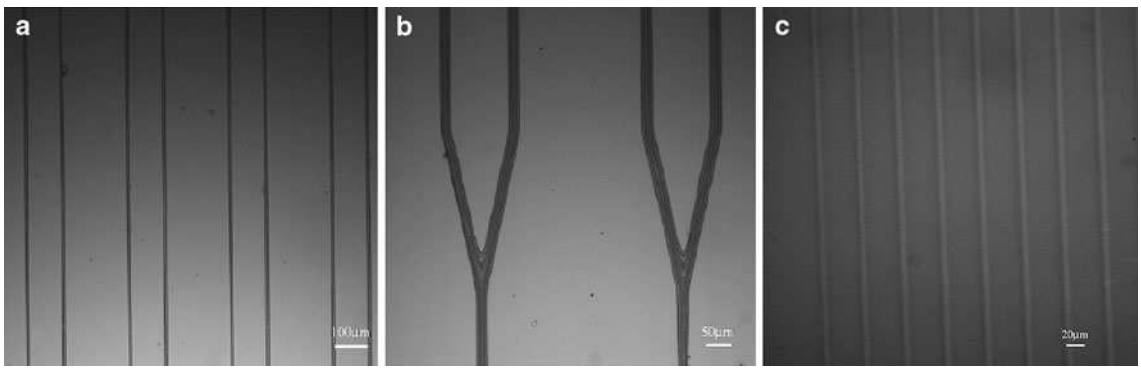

Fig. 5 Example of developed structures obtained by conventional UV lithography on a GPTMS-GeO_2 (molar ratio Si/Ge = 7/3) (**a**) a ridge waveguide, (**b**) a beam splitter. (**c**) Set of stripes achieved by direct UV lithography without developing step on a GPTMS-GeO_2 film. From ref [45]

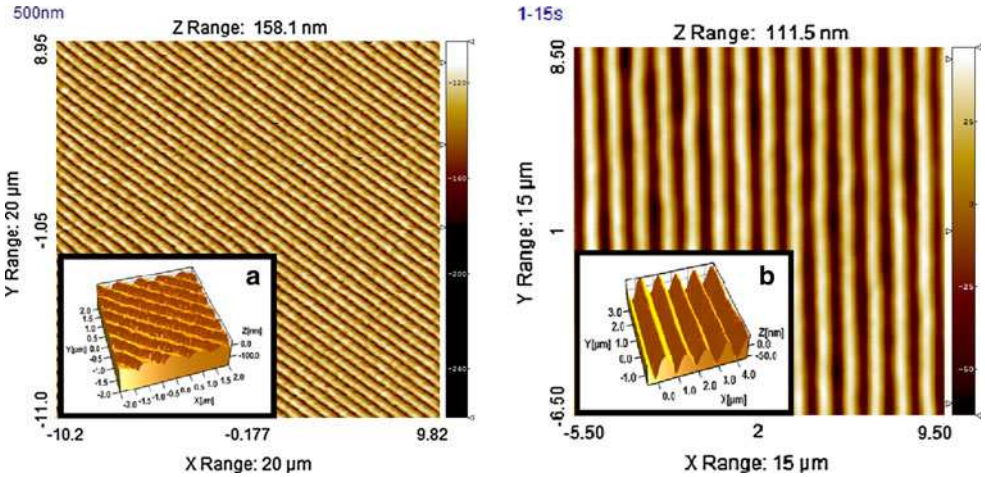

Fig. 6 AFM images of diffraction gratings with periods of 500 nm, field size 20×20 µm^2 (**a**) and of 1 µm, field size 15×15 µm^2, (**b**) fabricated with the two-beam interference system. In the *inset* the 3D images of zoomed scans of the patterns are showed

Since one of the aim of this study is to highlight the benefits of using HOI which in turn allow us to use a direct patterning process, for comparison, some patterned geometries obtained by the authors [50] on GPTMS-GeO_2 films with a traditional nano-lithographic procedure are shown in Fig. 7c and d. The process was performed using soft X-rays (1.5 keV from Synchrotron Light Source) on a pure commercial resist film (SAL) deposited on the GPTMS-GeO_2; after exposure to the X-rays beam with a mask, the SAL film was developed (in MF-322 industrial developer) and reactive ion etching (RIE) was performed (using a 1:2 volumetric mixture flux of Argon and CF4) to transfer the pattern on the underneath HOI sol–gel material. Residual SAL layer was then totally stripped away by means of hot acetone. As it can be observed in Fig. 7c and d, the obtained structures are rather well resolved in a depth of about 750 nm, but the roughness of the etched area is particularly evident. This fact, together with the time consuming and expensive conventional technique used, constitutes a drawback justifying the requirement for novel materials and for a simplification of the fabrication processes for mass production of micro- and nano-nanodevices.

The mechanism of interaction of UV light and X-rays with the same HOI system was recently investigated, by analyzing the FTIR spectroscopy measurements of Fig. 8.

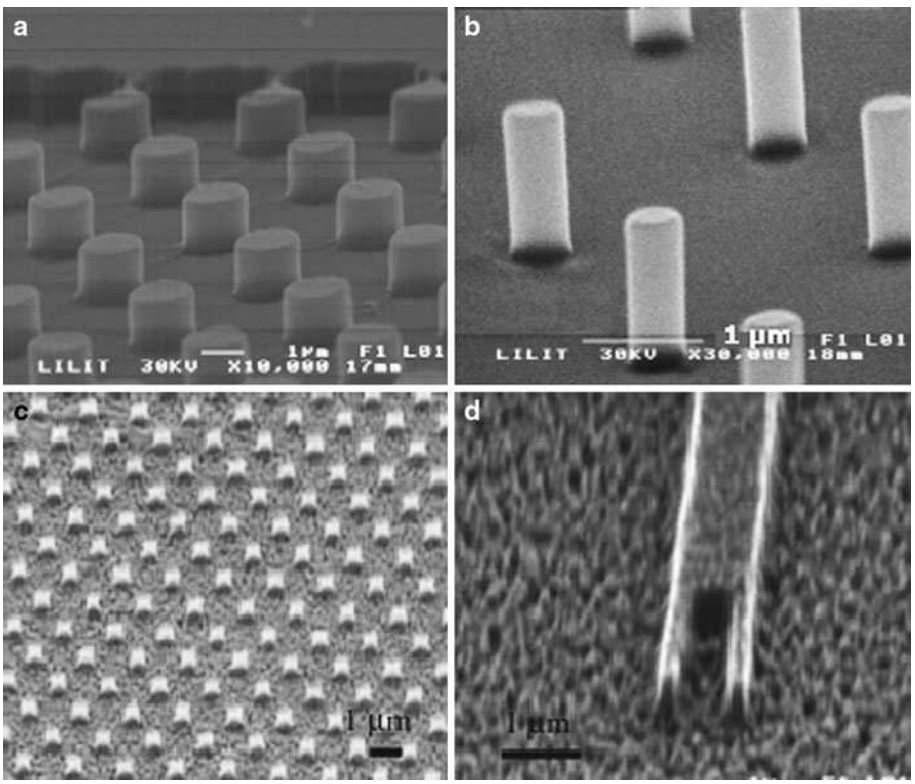

Fig. 7 XRL of a GPTMS-GeO_2 (molar ratio 8/2) film showing an array of pillars with diameter of 1.5 µm (**a**), from ref [38], and with pillar of lower dimension, 500 nm, and higher aspect ratio of about 3 (**b**), from ref [46]. The SEM images in (**c**) and (**d**) report some patterned geometries on the GPTMS-GeO_2 (molar ratio 8/2) system by the conventional XRL through the use of a polymer resist and the etching step

The FT-IR spectra show that to a first approximation the effect of UV and X-rays on the film structure modification is very similar, producing the epoxy curing (C–H stretching at 3,060–2,995 cm^{-1} and epoxy vibration at 910 cm^{-1} almost disappear) and organic degradation, evidenced by the increasing of a band at 1,750 of C=O species and of the broad 3,440 cm^{-1} band due to C–OH formation and/or H bonded water. The increasing of OH content is observed only in the case of X-rays exposure; before irradiation mainly Si–OH species are present (this contribution to OH band is centred at lower wavenumber, around 3,390 cm^{-1}); after exposure the band is shifted to higher wavenumber, around 3,440 cm^{-1} suggesting a predominant contribution from C–OH. In the case of UVL, these species are already present before irradiation, probably caused by the photo-initiator addition.

The organic degradation reasonably occurs on the more labile organic species such as the CH_2–O–CH_2 etheric bonds in the propylic chain, revealed by the decreasing of C–O–C stretching at 1,100 cm^{-1}; however, the intensity decrease and broadening of this peak may also be due to the epoxy polymerization that modifies the organic moieties structure. Even though the exposure doesn't produce carbonyl formation, as it will be shown later in the case of EBL, the broadening and decreasing of the C–O–C bond is still observed, suggesting that other species degrade during irradiation.

Several studies reported by the authors demonstrated that HOI GPTMS-GeO_2 system is directly patternable by EBL allowing to produce high resolution structures [34, 38, 51]. As in the case of XRL, by EBL the organic network formation occurs without the use of any photo initiator; in this way, all the problems related to the initiator diffusion [52, 53] and consequent loss of resolution and pattern quality are avoided.

In ref [34] the sensitivity of the resist, defined as the incident dose required to cause a change in the resist solubility sufficient for the production of a lithographically useful image, was estimated. The contrast is calculated as $\gamma = 1/\log(d_0/d_i)$, where d_0 is the dose required for 100% material remaining and d_i is the dose where the cross-linking starts to happen. Therefore, the contrast and the sensitivity can be obtained directly from a graph which relates the resist thickness and exposure, by plotting the normalized residual thickness of each exposed area, after development, versus the electron dose. Figure 9 shows the contrast curve achieved by using a micrometer test pattern in a film with a thickness of 350 nm. In particular, the influence of the post-exposure bake temperature on the resist contrast was investigated. As can be seen, the contrast was very similar for all the thermal treatments and it was only slightly reduced by increasing the post-exposure bake temperature, with a value changing from 2.5 to 2.2. An outstanding characteristic, highlighted by the Fig. 9, is the high sensitivity of this HOI system with a value around 5 μC/cm^2. In fact, the photospeed of a resist is a key point in industrial applications.

A comparison with two commercial resists (PMMA and SAL601) allows to minimize the influence of exposition parameters, evidencing the limits strictly due to the material structure. The achieved result on the GPTMS-GeO_2 HOI resist approaches those on commercial resists,

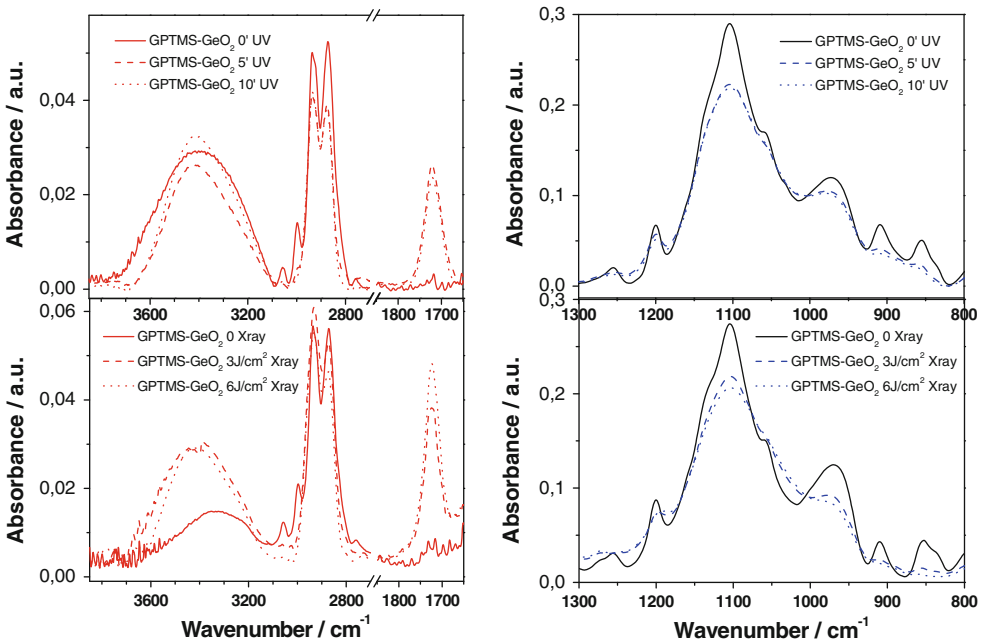

Fig. 8 Comparison between the interaction of UV and X-rays with the same HOI system, GPTMS-GeO_2 (molar ratio Si/Ge = 8/2)

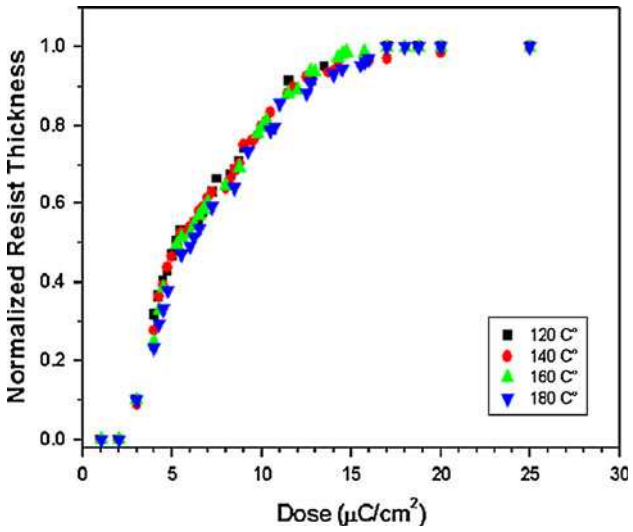

Fig. 9 Contrast curve for EBL direct patterning of GPTMS-GeO_2 (molar ratio Si/Ge = 8/2) as a different post-exposure bake temperatures. From ref [34]

showing features smaller than 100 nm (Fig. 10). The linewidth roughness is comparable with the other industrial products, and is so related to the performance of lithographic set up.

However, a remarkable property of this resist is its potential high resolution, as it was demonstrated in our more recent results; high resolution features were obtained by direct EBL for the production of a 2D DFB laser structure, as in the example of Fig. 11.

The other important quality of the HOI resists is that this class of materials can be easily functionalized, dispersing active compounds in the liquid phase during the synthesis process. Figure 12 shows the comparison of SEM micrographs of EBL fluorescent patterned films, doped with Rhodamine 6G, and the corresponding optical images of fluorescent structures. These results underline potential applications for the fabrication of integrated laser devices or photonic bandgap structures. In particular, the structure of Fig. 12b can work as a laser [54] and is based on the waveguiding action from a strip of doped hybrid film (refractive index $n = 1.51$) on top of a silicon dioxide surface ($n = 1.46$) surrounded by air; the geometry produces the total internal reflection of the light by the triangular ends of the structure, whose realization requires high resolution patterning. Figure 12b shows the desired structures obtained on a rhodamine 6G doped GPTMS-GeO_2 film by direct patterning.

The interaction of EB radiation with the HOI film, rarely investigated in literature, reveals a quite different and interesting behaviour respect the above described interaction with X-rays and UV. In particular, by micro FTIR analyses (Jasco micro FT-IR 620) small area pattern produced with EBL can be analysed (Fig. 13). In order to see the exposed structures the analysis was made after development of the film, and not just after irradiation as in the case of Fig. 8. The micro-FTIR spectra of films irradiated and developed were compared with FTIR spectra of UV exposed GPTMS-GeO_2 films (Ge/Si molar ratio of 2/8, synthesis reported in [34]), as shown in Fig. 13. Development was made by mixed solution of water/acetone in ratio 1:1 for 30 s after UV exposure and MF-319 for 20 s for EB exposed samples. From Fig. 13 it is evident that EB doesn't produce the degradation effect observed with both UV radiation and X-rays, because C=O absorption at 1,730 cm^{-1} is not here observed. As for UVL and XRL, EB exposure results in the epoxy polymerization, even without the addition of photo initiator; the polymerization causes the broadening of the C–O–C absorption at 1,100 cm^{-1}. As in the previous analyses, epoxy polymerization is confirmed by the decreasing of the absorption at 3,000 and 3,060 cm^{-1}, while the peak at 910 cm^{-1} seems to remain constant (see spectrum of the highest EB dose). However, this spectrum refers to developed films, i.e. the exposed film undergoes to a further treatment in aqueous basic medium. Also UV irradiated film of Fig. 12 was subjected to this development treatment, differently from the films of Fig. 8; in fact, it can be observed a slight increasing of the absorption at 910 cm^{-1}, comparing

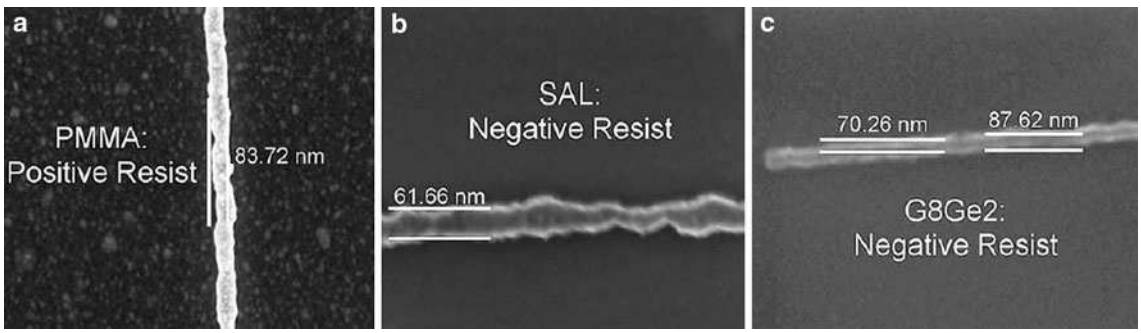

Fig. 10 Comparison of the ultimate resolution reached by using well-known commercial resists (**a**, **b**) and our hybrid sol–gel material, GPTMS-GeO_2 (molar ratio Si/Ge = 8/2) (**c**) in the same lithographic conditions. From ref [34]

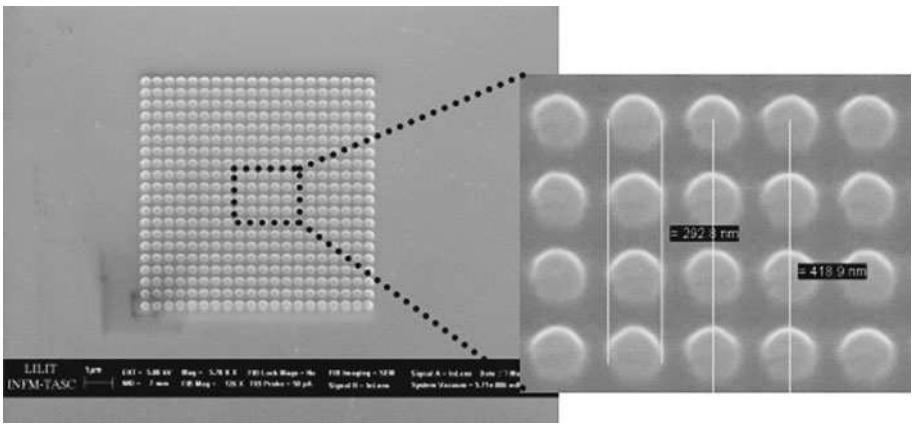

Fig. 11 SEM images of a square array of pillars patterned by EBL on the GPTMS-GeO_2 (molar ratio Si/Ge = 8/2) films. Pillars of 293 nm diameter possess a period 420 nm and a depth of 100 nm. From ref [63]

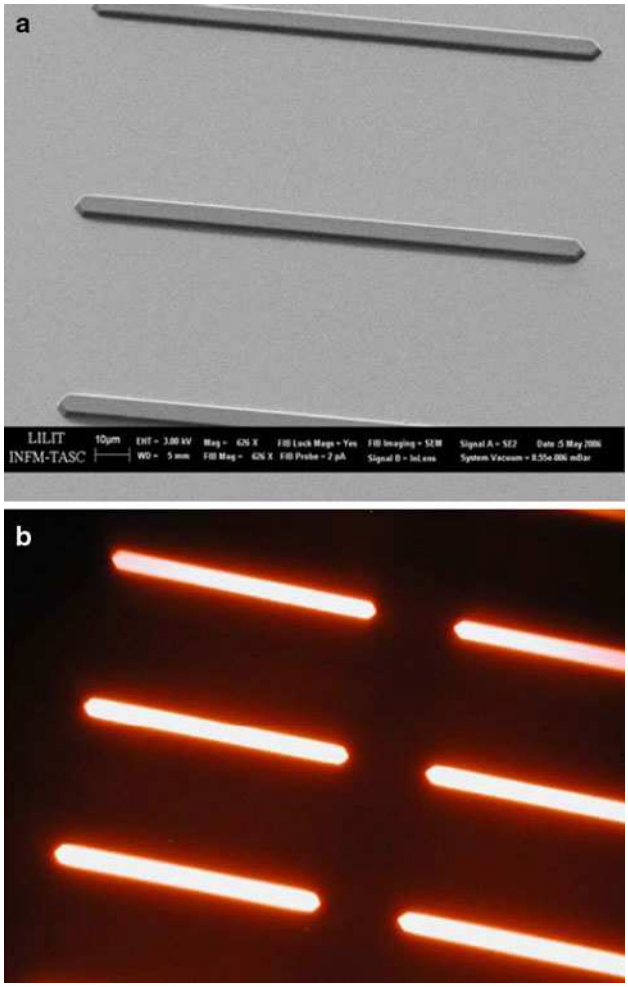

Fig. 12 Examples of patterned structures achieved by EBL on Rh6G doped GPTMS-GeO_2 films. The figure shows (**a**) the SEM image and (**b**) the fluorescence of the structures. From ref [51]

exposed and developed film, that can be due to the formation of Si–O^-. Moreover, in both EB and UV exposed and developed films the absorption at 960 cm^{-1} clearly decreases. The most probable hypothesis is that the basic etching removes preferentially GeO_2 aggregates, which absorption is just located at 960 cm^{-1}.

1.3 HOI materials based on GPTMS-GeO_2 and GPTMS-ZrO_2 for nano imprinting

Up to this point, the discussion clearly reveals how several lithographic processes take advantage from these smart materials. Thanks to their intrinsic nature which summarizes in the same network the features of polymers and inorganic materials, HOI systems can be successfully exploited even in the nanoimprinting technologies.

Nanoimprint lithography (NIL) is a relatively recent approach in the nanofabrication field and has been introduced in the 1995 by Chou's group [55, 56]. The striking and simple idea behind such techniques is the replication on a polymer film of the surface features of a stamp, just by the application of a pressure, assisted by the temperature or/and UV radiation. This simple approach is a low cost and scalable pattern transfer process and is not affected by diffraction problems, scattering effects or secondary electrons. For these reasons, NIL gained an increasing interest in the scientific field in view of its potential industrial impact [57–59].

As in the other lithographic techniques, polymers are the standard materials; but in last years [60–62] HOI sol–gel systems revealed to be very competitive due to the compositional versatility and functional properties.

The UV sensitivity of the previously described HOI has been exploited by the authors, also in the UV-NIL processes. UV-NIL avoids possible thermal limitations imposed by the substrate and usually requires less time and lower pressure ($\sim$1 bar) to obtain high quality replicas than the thermal version.

Figure 14 reports an example of a grating with a period of 4 μm on a GPTMS-GeO_2 film (molar ration 7/3) by UV-NIL. The imprinted features have been obtained using an elastomeric stamp, and by the addition of a cationic

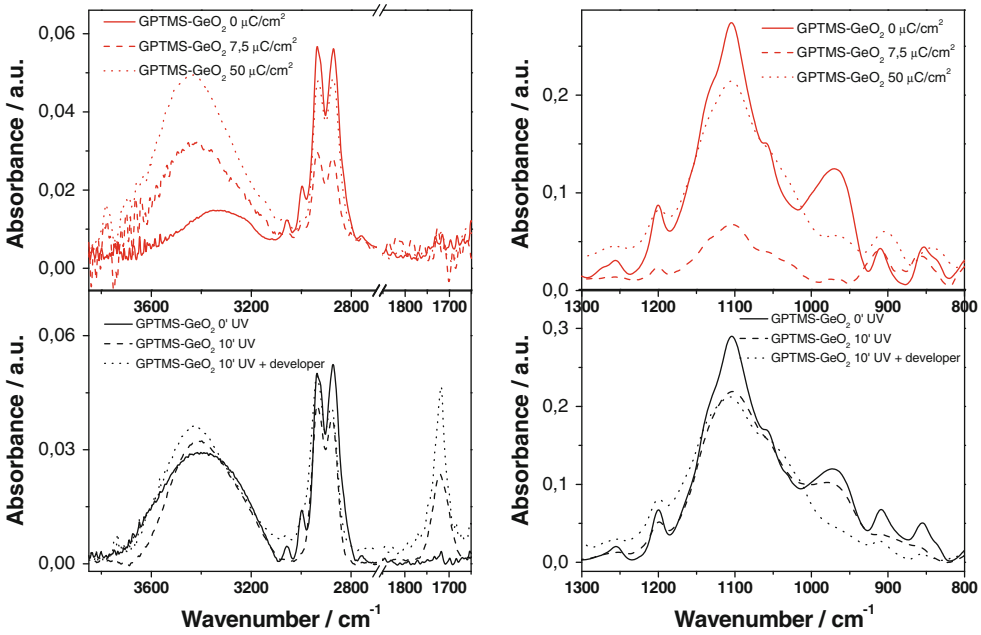

Fig. 13 Comparison between the micro-FTIR spectra of GPTMS-GeO2 films irradiated with EB and developed in a basic aqueous solvent and the FTIR spectra of the UV exposed films of the same HOI system

initiator to the epoxy sol–gel system, like in the case of conventional UVL [43].

The photopolymerization process together with the mechanical deformability of the HOI system, in the gel state, allow the replica of pattern with high fidelity. The UV exposure, through the transparent mold, hardens the HOI material, freezing the print of the stamp on the GPTMS-GeO_2 film surface. The grating in Fig. 14 appears homogenous and defect–free on a large area. Figures 15 show another application of UV-NIL to the same GPTMS-GeO_2 system to realize microfluidic device. This micrometric pattern is more complex than the periodic grating, presenting a variety of features with very different size.

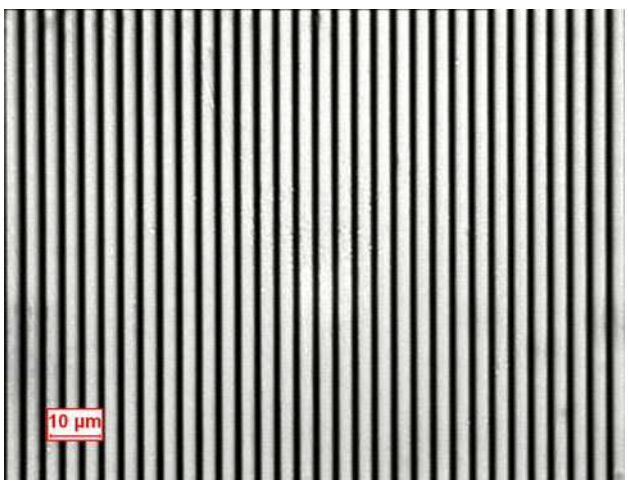

Fig. 14 Optical microscopy of a grating pattern with period of 4 μm realized by UV imprinting with a PDMS mold on the GPTMS-GeO_2 (molar ratio Si/Ge = 7/3) films

The optical microscopy in Fig. 15b demonstrates the ability of sol–gel HOI materials to get high quality imprinted structures.

The elastomeric molds used in these examples are made by polydimethylsiloxane (PDMS, Sylgard 184) which is highly transparent to the UV light and has good duplication capability; anyway the use of these soft stamps is low cost, but limited in high resolution pattern: nanometric features tend to collapse or stitch to each other (Fig. 16) and lateral distortions and structure deformation problems occur during the imprinting process. These drawbacks can be overcome by the use of more expensive hard stamps (quartz), or transparent substrates.

To further expand the range of imprintable HOI systems, with advanced and specific properties, the authors also discuss the application of T-NIL to different HOI materials. In such case, the sol–gel systems can be not necessarily UV sensitive. In the following, some examples of the obtained results are reported.

The GPTMS-GeO_2 system (molar ratio 8/2) has been successfully patterned by T-NIL, thanks to the peculiarity of sol–gel materials to harden with temperature (Fig. 17). The 1D periodic structures have been realized by T-NIL with a silicon master having a period of 406 nm and features depth of 200 nm. The grating replication has been performed with the application of a pressure of 3 kN and treating the sample at 120 °C during the imprinting procedure. As shown in Fig. 17, the realized samples have a high quality pattern over an area of 2 × 2 cm^2, and there is no evidence of the problems typical of the soft stamp with nanometric features. Moreover, the refractive index of GPTMS-GeO_2 system and the geometrical parameters of

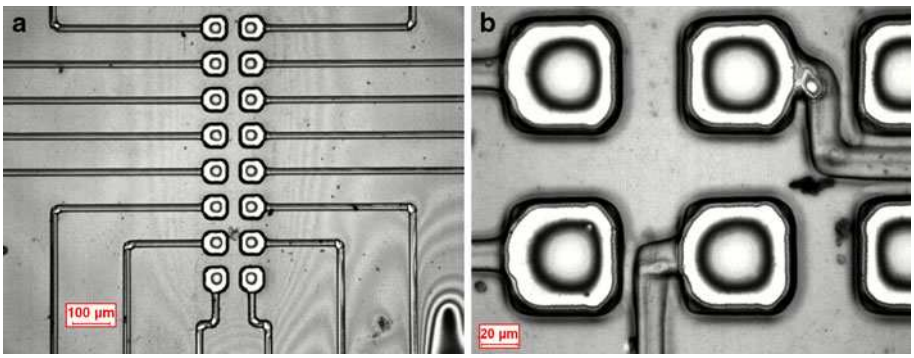

Fig. 15 (**a**) Optical microscopy of microfluidic device patterns realized by UV imprinting with a PDMS stamp on the GPTMS-GeO_2 (molar ratio Si/Ge = 7/3) films. In the figure (**b**) a magnification of the microfluidic features is reported

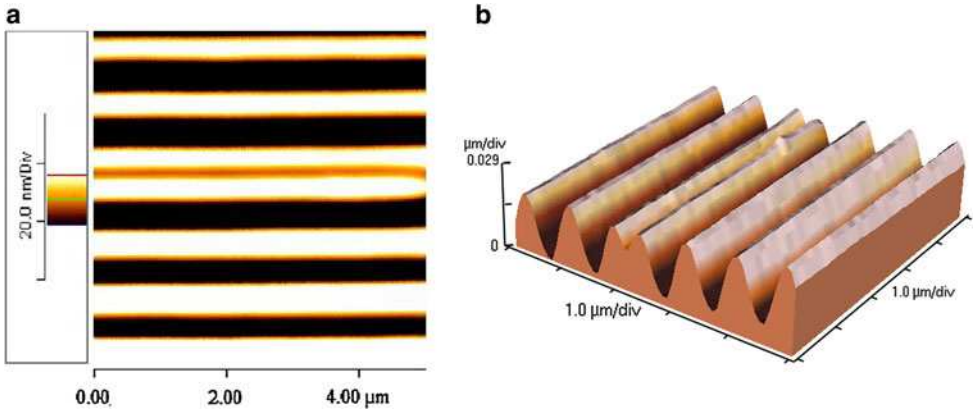

Fig. 16 AFM images (**a**) top view (**b**) 3D view of a 5 × 5 μm^2 area of a grating with period 406 nm. The pattern has been realized by UV imprinting with a PDMS mold on the GPTMS-GeO_2 (molar ratio Si/Ge = 7/3) films. It's clear the stitching of grating lines

the gratings have been tailored to realize a Distributed Feedback (DFB) laser. The deposition of an active sol–gel layer, doped with quantum dots, on such grating allowed to obtain a lasing emission around 620 nm [63]. The corrugation formed at the interface, between the active layer and the GPTMS-GeO_2, periodically modulates the effective refractive index, with a pitch of 406 nm; this kind of structure allows to feedback the light at a set wavelength, depending on the period [64, 65].

It's worth underlying that in the case of the application of T-NIL to UV sensitive materials, like the GPTMS-GeO_2 system, the epoxy ring has been preserved after the imprinting process. Therefore, these organic functionalities can be polymerized in a second step, giving the chance to combine different lithographic techniques and to design more complicated structures.

Another outstanding characteristic of these HOI systems is their high optical quality and transparency which has been exploited in the realization of UV transparent micrlolenses [66]. Figure 18a shows the UV–VIS spectra of two GPTMS based systems deposed on fused silica. In such application, the key point has been the selection of right precursors to obtain the lowest absorption in the deep UV region. GPTMS together with Germanium and Zirconium metal alkoxides revealed to be a good choice, showing a high transparency in the desired range, even for very thick

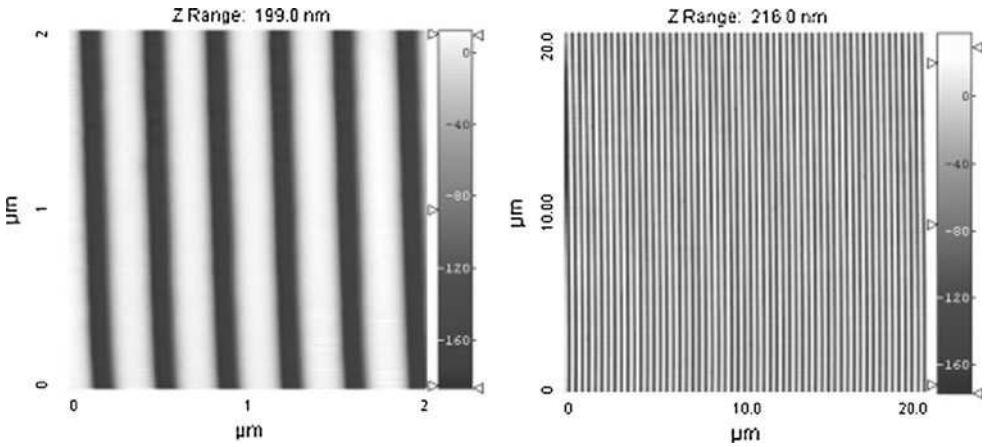

Fig. 17 AFM images of a grating pattern with period 406 nm realized by thermal imprinting on the GPTMS-GeO_2 (molar ratio Si/Ge = 8/2) films. The periodically structured surface acts as a 1D diffraction grating for a DFB laser. From ref [63]

films (60–110 μm). Alternative hybrid precursors like methacrylic and phenyl organically modified alkoxides suffer of absorption down 300 nm, due to the presence of substituted carbonyl groups and the π–π^* transitions in the aromatic ring, respectively [67, 68].

Such epoxy sol–gel materials present a 50% of transmission until 240 nm, especially in the case of GPTMS-GeO_2 films. The GPTMS-ZrO_2 system shows a weak absorption around 310 nm in a very thick sample, but maintains a transparency of 60% at 260 nm. However, GPTMS-ZrO_2 has better mechanical properties and dimensional stability respect to the GPTMS-GeO_2, important characteristics in the nanoimprinting technology. In fact, in the GPTMS-ZrO_2 system the organic polymerization already occurs during the synthesis step. The presence of zirconium precursor, a Lewis acid, polymerizes the epoxy ring in solution, giving a more crosslinked network. The FT-IR spectra of the two systems, GPTMS-GeO_2 and GPTMS-ZrO_2 allow to point out the main differences in the structure (Fig. 18b); as above mentioned, the bands at 3,000–3,060 cm^{-1} are characteristic of the epoxy rings and these peaks are still present in the GPTMS-GeO_2 and absent in the GPTMS-ZrO_2, confirming the epoxy ring opening reaction in presence of a stronger Lewis acid, the precursor of ZrO_2, respect to the GeO_2 one. Moreover, the broad band around 3,400 cm^{-1}, ascribed to OH groups absorption, is more pronounced in the GPTMS-GeO_2 system, indicating a less condensed inorganic network. As we have experimentally experienced during the imprinting process, the GPTMS-GeO_2 requires higher temperatures (around 120–150 °C) or treatment time in order to consolidate the structure and firmly maintain the pattern features.

Figure 19 reports some examples of high quality microlens arrays obtained on a large area, with both the hybrid sol–gel systems. Cylindrical and spherical sol–gel lenses have been achieved with different geometrical parameters, showing the possibility to tune the focal length (f) in a wide interval.

Microoptical elements with enhanced transmission in the deep UV can be key components in specific applications such as in photovoltaics as concentrators [69], or in light trapping systems suited for organic solar cells [70].

Figure 20 presents other micro and nanometric patterns obtained by T-NIL on the GPTMS/ZrO_2 system (molar ratio 8/2). The periodic gratings appear very well definite, even by using a low thermal treatment temperature (around 80 °C), during the imprinting process (Fig. 20b). In this way plastic substrates, usually sensitive to the temperature, can be also used.

The results highlight the broad possibilities derived from the control of the organic and inorganic polymerization and the challenges that this approach offers in the NIL techniques.

A relevant application, which nowadays gathers the interest in scientific community, is the realization of anti-reflective coatings (AR) [71, 72], so the authors exploit the NIL techniques and the versatility shown by the HOI sol–gel systems to reach the target.

When the incident radiation crosses the interface between two materials, reflectance losses are produced due to the different refractive index between the layers. In the case of common soda-lime glass, the reflection between air/glass interface is around 8%. Several strategies have been developed to increase the transmitted light, such as the single layer interference coating with a specific refractive index and thickness [73] suitable for a precise wavelength or a multilayer approach to widen the frequencies range [74]. The fundamental principle is to create a refractive index gradient between the environment and the substrate.

T-NIL has been exploited to realize a graded index pattern on a GPTMS-ZrO_2 film (Fig. 21b). Thanks to the low imprinting temperature required by this system, the coating has been deposited on a soda-lime glass and a PMMA slab and the pattern has been achieved by a nickel stamp (NIL technology, NILT) on an area of about 7 × 7 cm^2. The refractive index of the HOI sol–gel material has been matched with the one of the glass

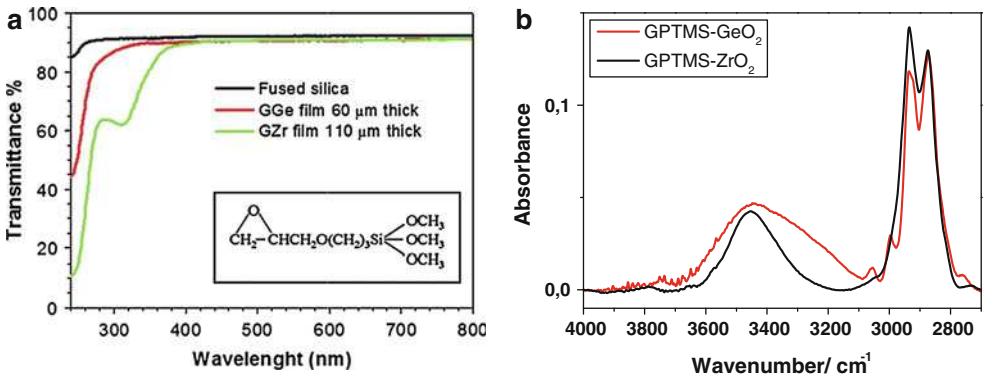

Fig. 18 (**a**) UV–Visible transmittance spectra of GPTMS based hybrid sol–gel materials, showing high transparency in the UV region. In the *inset* the molecular formula of GPTMS is shown, from ref [66], (**b**) FT-IR spectra of the GPTMS-GeO_2 (molar ratio Si/Ge = 8/2) and GPTMS-ZrO_2 (molar ratio Si/Zr = 8/2) systems just after the deposition

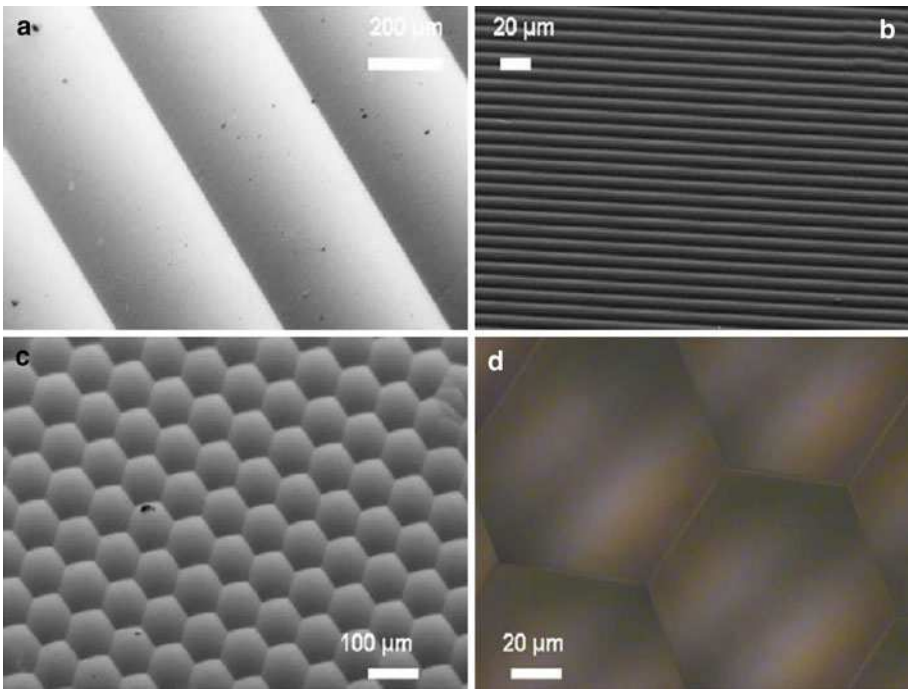

Fig. 19 SEM images of cylindrical microlenses with 400 µm (**a**) and 10 µm (**b**) of period. Triangular array of spherical lenses with 80 µm of period imaged by SEM (**c**) and optical microscopy (**d**). From ref [70]

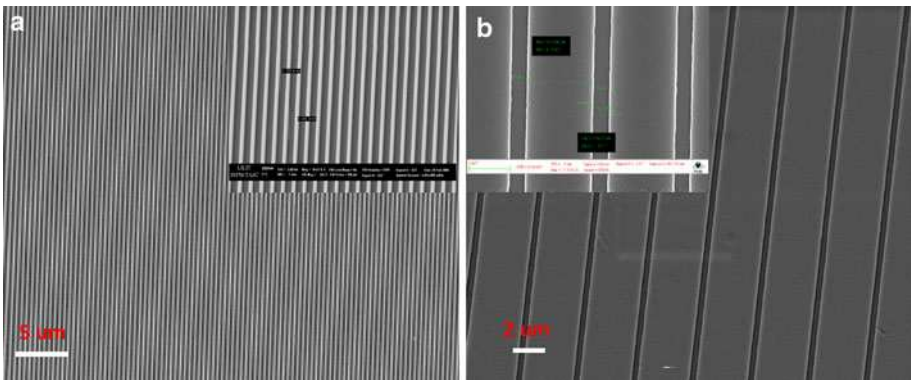

Fig. 20 SEM images of grating patterns with a period (**a**) of 4 µm and (**b**) of 500 nm realized by thermal imprinting on the GPTMS-ZrO_2 films

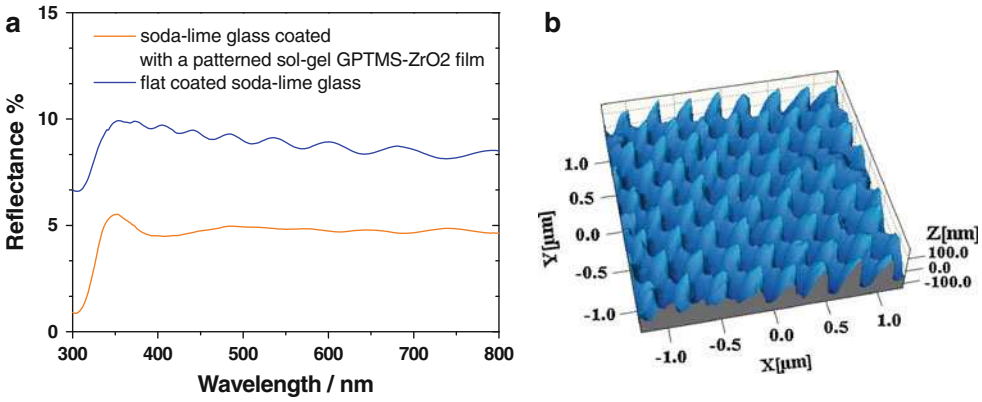

Fig. 21 (**a**) UV-VIS spectra of a glass slab coated with a flat GPTMS-ZrO_2 film and a thermal imprinted GPTMS-ZrO_2 film (**b**) AFM image of the antireflective pattern obtained on the hybrid sol–gel coating

substrate (around 1.51–1.52) to optimize the effect of the AR layer.

To assess the optical performances of the imprinted coating, the reflectance has been measured by means of a UV–Vis spectrometer, equipped with an integrating sphere. In Fig. 21a the reflection of a glass coated with the patterned GPTMS-ZrO_2 sol–gel film (refractive index around 1.51 at 600 nm) has been compared with a flat coated glass

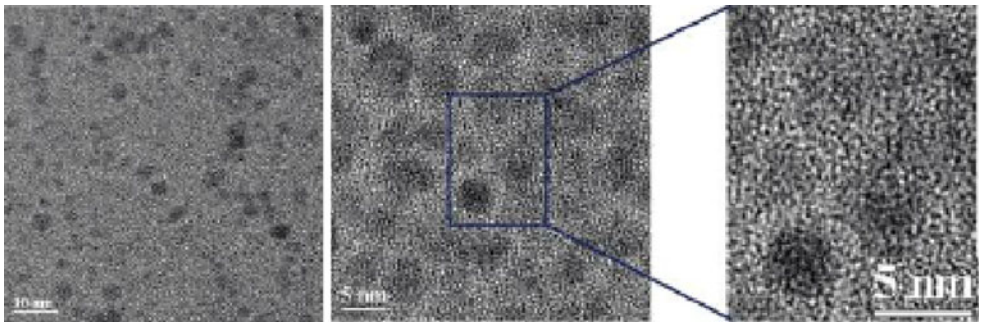

Fig. 22 TEM analysis of GPTMS-TiO_2 films (molar ratio Si/Ti = 7/3. From ref [76]

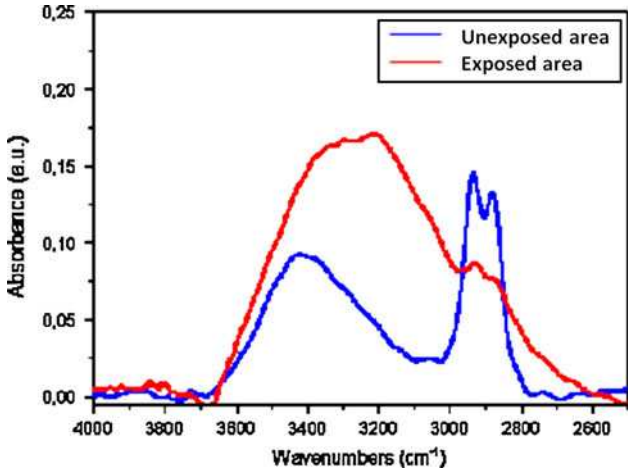

Fig. 23 Micro-IR spectra of the GPTMS-TiO_2 film after the exposition with the UV-photomask, where the decomposition of the organic species component is clearly visible from the decreasing of the peaks at 2,800–3,000 cm^{-1}. From ref [77]

in a range between 300 and 800 nm. The presence of the structured sol–gel film clearly reduces the reflection losses almost totally in all the visible range.

This phenomenon should be reduced to the minimum value, for example, to increase the performance of solar cells [75, 76], so the realization of efficient AR coatings is still a central issue. The results obtained in our groups demonstrate the reliability of HOI sol–gel materials to produce high quality AR coatings on a large area and their applicability in different fields.

1.4 HOI materials based on GPTMS-TiO_2

By changing the inorganic oxide component, a new material and patterning strategy have been reported [77, 78]. A hybrid GPTMS-TiO_2 system is prepared by a synthesis protocol described in [78], which allows to produce TiO_2 crystalline clusters in brookite form, without any thermal treatment (Fig. 22).

The presence of the crystalline TiO_2 domains results in the photosensitivity of the films, that can be patterned if exposed through a quartz photo-mask, thanks to the induced decomposition of the organic components of the system. Micro-FTIR spectrum of Fig. 23 collected on the exposed part of the film clearly shows the decomposition of the organic species as indicated by the decreasing of the peaks at 2,800–3,000 cm^{-1}.

In Fig. 24, SEM images of UV irradiated films, showing micrometric structures can be observed; the mask used for the exposure presents few different patterns: linear and ring gratings with periods in the range 40–150 μm.

Photosensitive TiO_2 containing HOI material has been also used for fabrication of microoptical elements by NIL [79]. The main difficulty in NIL occurs when highly

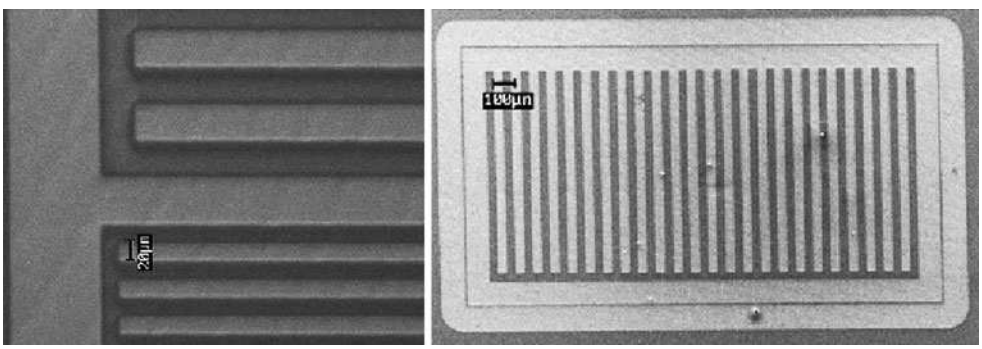

Fig. 24 Example of micrometric structures obtained by direct UV lithography on a GPTMS-TiO_2 (molar ratio Si/Ti = 7/3) film, without the developing step

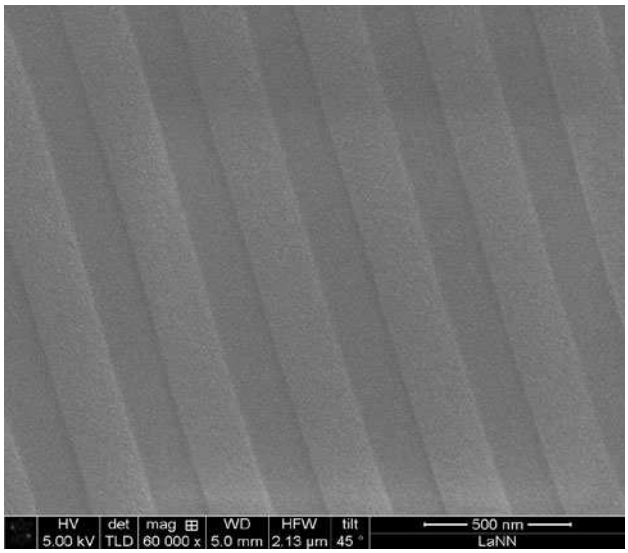

Fig. 25 SEM image of a Bragg grating achieved by T-NIL on a GPTMS-TiO_2 film, with a very high content of titania (molar ratio Si/Ti = 1/9)

inorganic systems have to be patterned, such as in the case of films with high refractive index. Recent results that we obtained demonstrate that GPTMS-TiO_2 HOI films with a TiO_2 content up to 90% (molar ratio respect to silica) can be patterned by NIL, allowing to achieve patterned films with refractive index up to 1.84 at 600 nm. This refractive index value is reached after UV exposure (dose around 30 J/cm^2) of the imprinted features, that makes the film completely inorganic and allows to well densify the structures. An example of NIL on a GPTMS-TiO_2 film (thickness 0.8 micron) achieved by using a periodic Si master (period 400 nm, duty cycle 50%) is shown in Fig. 25.

2 Conclusions

This review was intended to illustrate the opportunities offered by HOI, in particular by GPTMS based HOI materials, and their extreme interest for micro- and nano-lithography, opening the way for the realization of innovative resist materials. The reported results and recent achievements showed as through the choice of the synthesis protocol, photoinitiators and inorganic oxide precursors, a broad number of materials and lithographic processes may be derived that may satisfy various requirements for both applications and processes.

Acknowledgments The authors gratefully acknowledge support from the University of Padova through the PLATFORMS strategic project "PLAsmonic nano-Textured materials and architectures FOR enhanced Molecular Sensing"—prot. STPD089KSC.

References

1. Lebeau B, Innocenzi P (2011) Chem Soc Rev 40(2):886–906
2. Copuroglu M, O'Brien SM, Crean G (2006) Polym Degrad Stab 91:3185–3190
3. Passinger S, Saifullah MSM, Reinhardt C, Subramanian KRV, Chichkov BN, Welland ME (2007) Adv Mater 19:1218–1221
4. Briche S, Riassetto D, Gastaldin C, Lamarle C, Dellea O, Jamon D, Pernot E, Labeau M, Ravel G, Langlet M (2008) J Mater Sci 43:5809–5822
5. Prosposito P, Casalboni M, Orsini E, Palazzesi C, Stella F (2010) Solid State Sci 12:1886–1889
6. Fukushima M, Yanagi H, Hayashi S, Suganuma N, Taniguchi Y (2003) Thin Solid Films 438/439:39–43
7. Obi S, Gale MT, Kuoni A, De Rooij N (2004) Microelectron Eng 73/74:157–160
8. Saifullah MSM, Dae-Joon Kang, Subramanian KRV, Welland ME (2004) J Sol-Gel Sci Technol 29:5–10
9. Cheong WC, Yuan XC, Koudriacho V, Yu WX (2002) Opt Express 10(14):586
10. Grigorescu AE, Hagen CW (2009) Nanotechnology 20:29
11. Di Fabrizio E, Romanato F, Cabrini S, Kumar R, Perennes F, Altissimo M, Businaro L, Cojac D, Vaccari L, Prasciolu M, Candeloro P (2004) J Phys 16:33
12. Liang X, Morton KJ, Austin RH, Chou SY (2007) Nano Lett 7(12):3775
13. Rao J, Winfield R, Keeney L (2010) Opt Commun 283:2446–2450
14. Escarré J, Soderstrom K, Battaglia C, Haug FJ, Ballif C (2011) Sol Energy Mater Sol Cells 95:881–886
15. Kim KD, Jeong JH, Park SH, Choi DG, Choi JH, Lee ES (2009) Microelectron Eng 86:1983–1988
16. Buestrich R, Kahlenberg F, Popall M, Dannberg P, Muller-Fiedler R, Rosch O (2001) J Sol–gel Sci Technol 20:181–186
17. Moujoud A, Saddiki Z, Touam T, Najafi SI (2002) Thin Solid Films 422:161–165
18. Etienne P, Coudray P, Porque J, Moreau Y (2000) Opt Commun 174:413
19. Jung JI, Park OH, Bae BS (2003) J Sol-Gel Sci Technol 26:897–901
20. Coudray P, Etienne P, Moreau Y (2000) Mat Sci In Smicnd Proc 3:331–337
21. Popall M, Buestrich R, Kahlenberg F, Andersson A (2000) Mater Res Soc Symp Proc 621:CC9.4.1–CC9.4.12
22. Le Guevel X, Palazzesi C, Proposito P, Della Giustina G, Brusatin G (2008) J Mater Chem 18:3556–3562
23. Jabbour J, Calas-Etienne S, Smaıhi M, Gatti S, Kribich R, Pille G, Moreau Y, Etienne P (2007) Appl Surf Sci 253:8032–8036
24. O'Brien S, Copuroglu M, Crean GM (2007) Appl Surf Sci 253:7969–7972
25. Croutxe-Barghorn C, Belon C, Chemtob A (2010) J Photopol Sci Technol 23(1):129–134
26. Que W, Jia CY, Sun M, Sun Z, Wang LL, Zhang ZJ (2008) Opt Express 16(6):3490–3495
27. Binh NT, Thanh NT, Trung DT, Huong NT, Minh LQ (2008) J Korean Phys Soc 52(5):1501–1505
28. Luo X, ZHA C, Luther-Davies B (2005) Opt Mater 27:1461–1466
29. Que W, Hu X, Zhang QY (2003) Chem Phys Lett 369:354–360
30. Oubaha M, Copperwhite R, Murphy B, Kolodziejczyk B, Barry H, O'Dwyer K, MacCraith BD (2006) Thin Solid Films 510:334–338
31. Segawa H, Yamaguchi S, Yamazaki Y, Yano T, Shibata S, Misawa H (2006) Appl Phys A 83:447–451

32. Segawa H, Tateishi K, Arai Y, Yoshida K, Kaji H (2004) Thin Solid Films 466:48–53
33. Saifullah MSM, Subramanian KRV, Tapley E, Kang D-J, Welland ME, Butler M (2003) Nano Lett 3(11):1587–1591
34. Della Giustina G, Prasciolu M, Brusatin G, Guglielmi M, Romanato F (2009) Microelectron Eng 86:745–748
35. Brigo L, Pistore A, Grenci G, Carpentiero A, Romanato F, Brusatin G (2010) Microelectron Eng 87:947–950
36. Falcaro P, Malfatti L, Vaccai L, Amenitsch H, Marmiroli B, Grenci G, Innocenzi P (2009) Adv Mater 21:4932–4936
37. Brusatin G, Della Giustina G, Romanato F, Guglielmi G (2008) Nanotechnology 19:175306
38. Park HH (2011) Microelectron Eng 88:923–928
39. Peroz C, Chauveau V, Barthel E, Søndergard E (2009) Adv Mater 21:555–558
40. Lee TY, Guymon CA, Sonny Jonsson E, Hoyle CE (2004) Polymer 45:6155–6162
41. Srinivasan S, Lee MW, Grady MC, Soroush M, Rappe AM (2010) J Phys Chem A 114:7975–7983
42. Della Giustina G, Brusatin G, Guglielmi M, Palazzesi C, Orsini E, Prosposito P (2010) Solid State Sci 12:1890–1893
43. Crivello JV, Lam JHW (1980) J Polym Sci Polym Chem Ed 18:2697–2714
44. Della Giustina G, Brusatin G, Guglielmi M, Palazzesi C, Orsini E, Proposito P (2010) Solid State Sci 12:1890–1893
45. Della Giustina G, Brusatin G, Guglielmi M, Romanato F (2007) Mater Sci Eng C 27:1382–1385
46. Brusatin G, Della Giustina G, Guglielmi M, Innocenzi P (2006) Prog Solid State Chem 34:223–229
47. Guglielmi M, Brusatin G, Della Giustina GJ (2007) Non-Cryst Solids 353:1681–1687
48. Della Giustina G, Zacco G, Zanchetta E, Guglielmi M, Romanato F, Brusatin G (2011) Microelectron Eng 88:1923–1926
49. Buso D, Della Giustina G, Brusatin G, Guglielmi M, Martucci A, Chiasera A, Ferrari M, Romanato F (2009) J Nanosci Nanotechnol 9:1858–1864
50. Della Giustina G, Guglielmi M, Brusatin G, Prasciolu M, Romanato F (2008) J Sol-Gel Sci Technol 48:212–216
51. Patsis GP, Glezos N (1999) Microelectron Eng 46:359–363
52. Foucher J, Pikon A, Andes C, Thackeray J (2007) Proc SPIE 6518:65181Q
53. Balslev S, Romanato F (2005) J Vac Sci Technol B 23(6):1
54. Chou SY, Krauss PR, Renstrom PJ (1995) Appl Phys Lett 67:3114–3116
55. Chou SY, Krauss PR, Renstrom PJ (1996) Science 272:85–87
56. Schmitt H, Rommel M, Bauer AJ, Frey L, Bich A, Eisner M, Voelkel R, Hornung M (2010) Microelectron Eng 87:1074–1076
57. Ahn AH, Guo LJ (2009) ACS Nano 3(8):2304–2310
58. Pozzato A, Dal Zilio S, Fois G, Vendramin D, Mistura G, Belotti M, Chen Y, Natali M (2006) Microelectron Eng 83:884–888
59. Kim WS, Kim KS, Eo YJ, Yoon KB, Bae BS (2005) J Mater Chem 15:465–469
60. Letailleur A, Teisseire J, Chemin N, Barthel E, Søndergard E (2010) Chem Mater 22:3143–3151
61. Gale MT, Gimkiewicz C, Obi S, Schnieper M, Sochtig J, Thiele H, Westenhofer S (2005) Opt Lasers Eng 43:373–386
62. Fortunati I, Gardin S, Todescato F, Signorini R, Bozio R, Jasieniak JJ, Martucci A, Pistore A, Guglielmi M, Prasciolu M, Romanato F (2010) Nonlinear Opt Quantum Opt 41(1):73–86
63. Ye C, Wong KJ, He Y, Wang X (2006) Opt Express 15(3):936
64. Pisignano D, Persano L, Mele E, Visconti P, Anni M, Gigli G, Cingolani R, Favaretto L, Barbarella G (2005) Synth Met 153:237–240
65. Dal Zilio S, Della Giustina G, Brusatin G, Tormen M (2010) Microelectron Eng 87:1143–1146
66. Versace DL, Oubaha M, Copperwhite R, Croutxé-Barghorn C, MacCraith BD (2008) Thin Solid Film 516:6448
67. Sato N, Nagayama M, Yokoyama Q (2003) J Photopolym Sci Technol 16:679
68. Goetzberger A, Goldschmidt JC, Peters M, Löper P (2008) Sol Energy Mater Sol Cells 92(12):1570–1578
69. Dal Zilio S, Tvingstedt K, Inganäs O, Tormen M (2009) Microelectron Eng 86(4–6):1150–1154
70. Tohge N, Hasegawa M, Noma N, Kintaka K, Nishii J (2003) J Sol-Gel Sci Technol 26:903–907
71. Li X, Du X, He J (2010) Langmuir 26(16):13528–13534
72. Zhang X, Ye H, Xiao B, Yan L, Lv H, Jiang B (2010) J Phys Chem C 114(47):19979–19983
73. Chen D (2001) Sol Energy Mater Sol Cells 68:313–336
74. Chhajed S, Schubert MF, Kim JK, Schuber EF (2008) Appl Phys Lett 93:101914
75. Faustini M, Nicole L, Boissiere C, Innocenzi P, Sanchez C, Grosso D (2010) Chem Mater 22:4406–4413
76. Gardin S, Signorini R, Pistore A, Della Giustina G, Brusatin G, Guglielmi M, Bozio R (2010) J Phys Chem C 114:7646–7652
77. Gardin S, Della Giustina G, Brusatin G, Signorini R (2011) J Nanosci Nanotechnol 11(1):195–199
78. Park HH et al (2010) J Mater Chem 20:1921–1926
79. Yu W, Yuan X-C (2004) J Mater Chem 14:821–823